Photoacoustics 30 (2023) 100464

Contents lists available at ScienceDirect

Photoacoustics

journal homepage: www.elsevier.com/locate/pacs

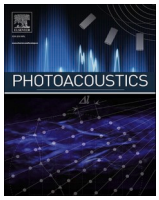

Surface plasmon-based detection for picosecond ultrasonics in planar gold-dielectric layer geometries

F. Noll [a,d], N. Krauß [a], V. Gusev [b], T. Dekorsy [a,c], M. Hettich [a,d,*]

[a] Department of Physics, University of Konstanz, 78464 Konstanz, Germany
[b] Laboratoire d'Acoustique de l'Université du Mans (LAUM), UMR 6613, Institut d'Acoustique - Graduate School (IA-GS), CNRS, Le Mans Université, Av. O. Messiaen, 72085 Le Mans, France
[c] Institute of Technical Physics, German Aerospace Center, Pfaffenwaldring 38-40, 70569 Stuttgart, Germany
[d] Research Center for Non-Destructive Testing GmbH (RECENDT), Altenbergerstr. 69, 4040 Linz, Austria

ARTICLE INFO

Keywords:
Picosecond ultrasonics
Acousto-plasmonics
Surface plasmon resonance (SPR)
ASOPS
Thin Films
Coherent Acoustic Phonons
Attenuated Total Reflection (ATR)

ABSTRACT

Longitudinal acoustic modes in planar thin gold films are excited and detected by a combination of ultrafast pump-probe photoacoustic spectroscopy and a surface plasmon resonance (SPR) technique. The resulting high sensitivity allows the detection of acoustic modes up to the 7th harmonic (258 GHz) with sub-pm amplitude sensing capabilities. This makes a comparison of damping times of individual modes possible. Further, the dynamics of the real and imaginary part of the dielectric function and the film's thickness variation are separated by using the dependence of the amplitudes of the acoustic modes on the detection angle and the surface plasmon resonance. We find that longitudinal acoustic modes in the gold films mainly affect the real part of the dielectric function and highlight the importance to consider thickness related effects in acousto-plasmonic sensing.

1. Introduction

Since its introduction in the 1980s picosecond ultrasonics [1,2] has proven to be a valuable tool for the investigation and control of acoustic dynamics in the GHz to THz frequency range. However, measurement of the accompanying small changes in optical or geometrical properties still poses a challenging task in many applications. Thus, different detection schemes have been employed during the last decades to tackle this issue and still foster an active development.

Widely used all-optical approaches currently include direct reflection/transmission experiments [3], interferometry either by external homo/heterodyning [4–6] or using Fabry Perot like sample geometries [7], beam deflection [8] and diffraction [9,10] schemes. Taking advantage of surface plasmons has resulted in a tremendous success in various sensing applications [11]. The special case of localized surface plasmons also plays a prominent role in the investigation of nanoparticle acoustics [12,13] due to the relaxed excitation requirements compared to other sample geometries. It is thus not surprising that attempts have been made to adopt surface plasmons for the detection in picosecond ultrasonic experiments in planar [14–17], grating [18,19] and nanostructured [20] geometries. Here, we combine the acousto-plasmonic detection via surface plasmon resonances with asynchronous optical sampling to explore the potential of this approach to access higher order acoustic eigenmodes in planar gold layers. We further discuss the influence of the acoustic dynamics on changes in the dielectric function and the importance of the so far mostly neglected thickness changes in the surface plasmon based detection in our sample geometry. We finally highlight some of the open questions we encountered in this study to stimulate further developments in acousto-plasmonic sensing schemes.

2. Methods

2.1. Surface plasmon polaritons

Surface plasmon polaritons (SPs) are coupled electromagnetic and electron density waves at a material interface which decay as evanescent waves in both materials [21]. One of the possibilities to excite SPs is the so called Kretschmann-configuration that uses a prism, coated with a metal film and an additional dielectric layer [22,23]. Here, p-polarized light that is incident under a specific angle will couple to the SPs which results in a strong angle dependent decrease of the reflected light intensity. The sample reflectance can be described by an explicit

Abbreviations: ASOPS, Asynchronous optical sampling.

* Correspondence to: Research Center for Non-Destructive Testing GmbH, Altenbergerstr. 69, 4040 Linz, Austria.
E-mail address: mike.hettich@recendt.at (M. Hettich).

https://doi.org/10.1016/j.pacs.2023.100464
Received 15 December 2022; Received in revised form 3 February 2023; Accepted 21 February 2023
Available online 23 February 2023

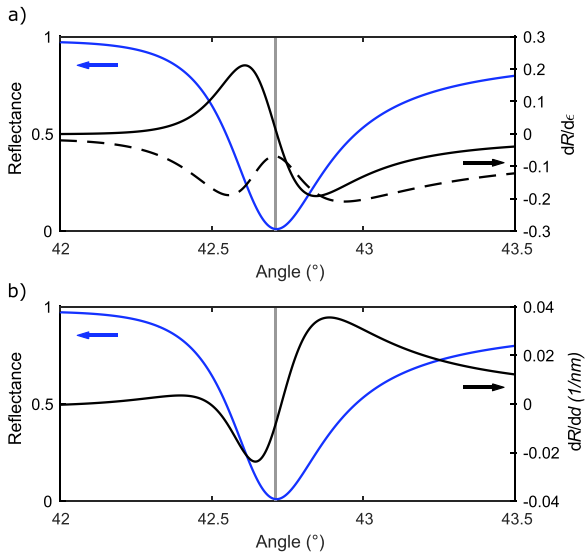

Fig. 1. Surface plasmon resonance for a layered system of glass/gold/air (left axis, blue line) and sensitivity of the SPR to the variation of (a) the real part (right axis, black line) and imaginary part (dashed black line) of the gold layer's dielectric function and (b) the gold layer's thickness. The vertical grey line marks the resonance angle.

three-layer model or a generalized transfer matrix approach [21] and shows a very sharp resonance, termed surface plasmon resonance (SPR), that strongly depends on the layer's permittivity, thickness and the angle of incidence. Figure 1(a) (blue line) shows the angle dependent reflectance calculated for a glass prism in air, covered by a gold film with 45 nm thickness for a wavelength of 785 nm with $\varepsilon = -22.9 + 1.4\mathrm{i}$ [24], $n_{\mathrm{air}} = 1$ and $n_{\mathrm{glass}} = 1.51$ [25]. For these parameters almost full coupling into the SP-mode with vanishing reflectance is achieved. Towards thinner or thicker films, the resonance becomes less pronounced and wider. The black lines depict the dependency of the reflectance R on changes to the gold film's dielectric function, where the solid line corresponds to changes of the real and the dashed line to changes of the imaginary part, respectively.

A change in the real part of the dielectric function mainly causes a shift of the resonance angle position, while a change in the imaginary part influences mainly the width and minimal reflectance. Depending on the combination of film thickness and imaginary part of the dielectric function, the local maximum of $\mathrm{d}R/\mathrm{d}\epsilon_{\mathrm{i}}$ at the resonance angle can reach positive or negative absolute values. The resonance is also strongly influenced by changes of the gold layer's thickness which is shown in Fig. 1(b).

Acoustic vibrations lead to strain η in the gold layer which results in a variation $\Delta\epsilon$ of the permittivity via the photoelastic coefficients $\mathrm{d}\epsilon/\mathrm{d}\eta$. This in turn causes a variation of the reflectance according to the shown derivatives. These derivatives are about one to two orders of magnitude above the ones from direct reflection at a gold/air interface ($\mathrm{d}R/\mathrm{d}\epsilon_{\mathrm{r}} \approx -1.5{\cdot}10^{-3}$, $\mathrm{d}R/\mathrm{d}\epsilon_{\mathrm{i}} \approx -1.6{\cdot}10^{-2}$). When detecting the relative change in reflectance $\Delta R/R$, the signal is further enhanced in the vicinity of the SPR-minimum due to the decreasing background reflectance R. However, due to zero crossings of $\mathrm{d}R/\mathrm{d}\epsilon_{\mathrm{r}}$ and $\mathrm{d}R/\mathrm{d}d$ close to the SPR minimum, this results in the maximum enhancement for ϵ_{r} and d being found at the slopes of the SPR and for ϵ_{i} at the slopes or minimum depending on the exact film parameters.

2.2. Samples

Half-cylindrical glass prisms (FOCtek, material H-K9L, same properties as N-BK7) were used to employ the Kretschmann-configuration. After an initial cleaning step with isopropanol and acetone the prisms were coated with gold films by thermal evaporation ($2-3$ nm/s at $4-7{\cdot}10^{-4}$ Pa). The layer thickness was controlled in-situ during deposition by a quartz crystal microbalance. Three samples with nominal gold film thicknesses of 30, 45 and 50 nm were produced. Additional adhesion promotion layers, like chromium or titanium, were omitted to keep the samples as simple as possible in terms of SPR and acoustic mode characteristics.

2.3. Pump-probe setup

A Ti:sapphire based asynchronous optical sampling system (ASOPS) with 1 GHz repetition rate [26,27] was used for the excitation of acoustic eigenmodes in the gold films and subsequent time-resolved monitoring of the acousto-plasmonic interaction. The beams were fiber coupled and the fiber outputs mounted on a rotational stage and a rotating arm for simple adjustment of the incidence angle. An optical pulse compressor was used to compensate for the fiber induced pulse broadening, resulting in a pulse width (FWHM) of less than 500 fs and a spectral width of 30 nm for the pump beam and 150 fs pulse width and 20 nm spectral width for the probe beam. Further system details are described elsewhere [28]. The pump and probe beams were tuned to center wavelengths of 815 nm and 785 nm with powers of 620 mW (0.62 nJ pulse energy) and 40 mW, respectively.

A schematic of the experimental setup is shown in Fig. 2(a). The pump beam was focused from the air side onto the gold layer to a spot with a diameter of approximately 30 μm. The probe beam was p-polarized by a half-wave-plate and polarizing beam splitter cube (PBS) and focused under the SPR-angle from the prism side onto the gold film to an ellipse with axes of approximately 15 and 20 μm. The curvature of the prism was compensated by a cylindrical lens. A part of the probe beam was split off and used for balanced detection to minimize the influence of laser noise. Because of the angle distribution in the focal cone of the probe beam, only a part of the beam fulfills the SPR condition as sketched in the inset of Fig. 2(b). We used a movable slit on a rotational stage to select and scan the angular response of the system. This approach has the advantage, that the angle of detection can be selected without introducing any change to the pump-probe-alignment. However, it results in an averaging over an angle range of about 10′ due to the slit width.

Since our probe pulse has a FHWM spectral bandwidth of about 20 nm we expect a broadening of all angle-resolved phenomena due to a weighted wavelength dependent response. This is mainly caused by the wavelength dependence of the gold film's dielectric function. We assume the photoelastic coefficients $\mathrm{d}\epsilon/\mathrm{d}\eta$ of the gold bulk material to be wavelength independent over the spectral width of the optical probe pulse. Since this approximation is reasonable but would still require an experimental verification, we suggest including an optical diffractive element for specific wavelength selection in the probe path in future experiments.

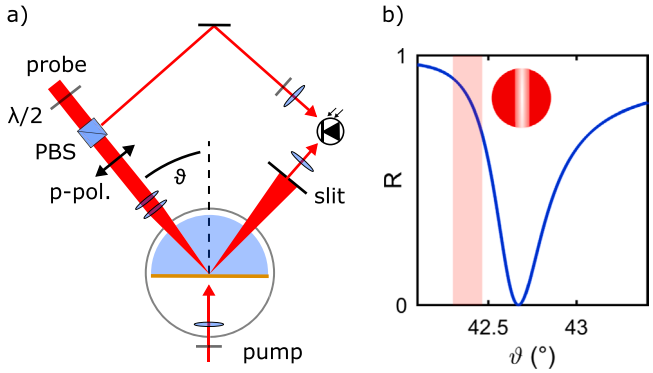

Fig. 2. a) Schematic of the experimental configuration. b) The surface plasmon resonance curve (blue line) is shown with the measured angle interval (shaded area) due to the finite slit width. The inset shows a sketch of the reflected probe beam's cross section.

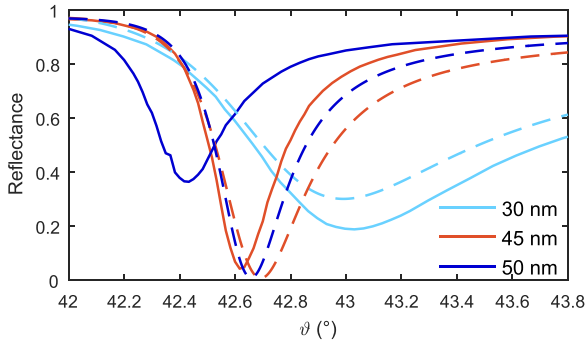

Fig. 3. Experimental (solid lines) and calculated (dashed lines) surface plasmon resonances of the three samples with different Au film thickness.

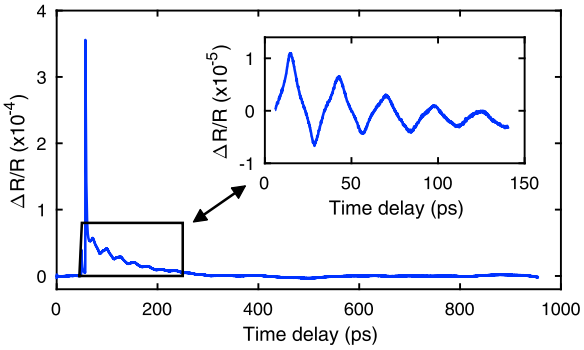

Fig. 4. Transient reflectivity of the 45 nm sample detected under SPR conditions. Inset: Extracted signal of the thickness oscillation of the gold film.

3. Results and discussion

3.1. SPR resonances

The angle dependent surface plasmon resonances of the samples were first measured in the static case and are shown in Fig. 3. The 45 and 30 nm sample showed results close to the calculated resonance curves with the permittivity of gold taken from Johnson and Christy [24]. Small shifts of the resonance angle can be explained by variations of the permittivity's real part and possible adsorbates on the gold's surface [22,29]. Please note that the resonance of the 45 nm sample is much narrower than expected from calculations. We have currently no conclusive explanation for this observation, since various possible errors would have the opposite effect, i.e., a broadened resonance. The 50 nm sample deviated significantly from the calculated curve, being much broader, less pronounced and shifted in resonance angle which hints to a higher SP damping and worse coupling to the SP mode. Certain deviations from literature values are to be expected because the permittivity and grain structure of evaporated films are known to depend strongly on deposition parameters [29]. However, this does not explain the results obtained for the 50 nm film, which we attribute to weaker adhesion and a possible deteriorated film quality because of aging, as it was the oldest sample at the time of the experiment. Since the 45 nm sample still shows a reasonable agreement with theoretical predictions and in particular the sharpest resonance and therefore the highest enhancement factor, we mainly focus on this sample in the further analysis.

3.2. Mode identification

Figure 4 shows a typical transient reflectivity signal of the time-resolved pump-probe measurement on the 45 nm sample in the vicinity of the SPR resonance angle. The initial sharp peak and the following decaying background are caused by the excitation of the free electron gas and subsequent electron-electron, electron-lattice and lattice thermalization in the gold film. The pump pulse photon energies are below the gold interband transitions. Superimposed on this background, damped oscillations are visible which are shown in more detail in the inset. Please note that also low frequency modes are present in the data that dominate the time traces at longer time delays. One of them is caused by time-domain Brillouin-scattering discussed later while the other modes are out of the scope of this work. The above-mentioned signal characteristics are present in the time-resolved measurements of all samples with varying sign, phase and amplitude depending on the angle of detection. The observed oscillation can be assigned to a longitudinal mode (thickness oscillation) of the gold film which is caused by the gradient of the thermo-elastic stress that is induced by the deposited pulse energy. Although the penetration depth of light in gold at the pump wavelength of 815 nm is only about 13 nm, with regard to the lattice overheated electrons can diffuse about 100 nm in gold before their energy is transferred to the lattice and therefore cause an almost homogeneous energy deposition along the axial direction of the film [30,31]. The acoustic impedance mismatch between gold and glass ($Z_{Au} = 62.5 > Z_{BK7} = 15.2$) results in an acoustic behavior of the film analogous to a free-standing membrane with stress free boundaries. Since the excitation spot size is large compared to the film thickness, the acoustic problem can be treated as one-dimensional. Thus, the frequencies of the modes of the thickness oscillation can be calculated as $f = n\nu_l/2d$ with the longitudinal sound velocity ν_l, the film thickness d and mode number $n \in \mathbb{N}$. For the given system odd harmonics, possessing symmetric distribution of strain relative to the middle plane of the film, are expected to be photo-excited, with a decreasing amplitude proportional to $1/n^2$. The even modes, possessing asymmetric strain distribution, are not photo-excited by the uniform and symmetric distribution of the photo-induced mechanical stress [7,32].

The acoustic breathing mode of the gold film was extracted by fitting and subtracting a double exponential decaying function for all sample thicknesses. Figure 5 shows the acoustic signals of the three films and the corresponding zero-padded Fourier spectra. All signals have been detected at the respective angle of maximum signal enhancement which is located at the slope on the smaller angle side of the SPR at about $\vartheta_{rel} = -4'$ depending on the sample. The spectrum of the 45 nm sample shows odd harmonics up to the 7th order (258 GHz), which is, to the best of our knowledge, the highest harmonic observed so far for a gold film/substrate configuration. The resulting average frequency of the fundamental mode ($n = 1$) was determined to 36.6 ± 0.5 GHz by a linear fit to the odd harmonics in the spectra of three different positions on the sample. With a nominal thickness of 45 nm this corresponds to a longitudinal sound velocity of 3.29 ± 0.05 km/s, which is in good agreement with the literature value of 3.24 km/s [16]. For the other samples, the oscillation was resolved up to the 5th (50 nm) and 3rd (30 nm) harmonic and the sound velocities were determined to 3.32 ± 0.05 km/s and 3.30 ± 0.03 km/s, respectively. The spectra of the 45 and 50 nm films show small contributions at frequencies corresponding to or close to the second and fourth harmonic, which possibly stem from a not completely homogeneous, i.e., symmetrical relative to the middle plane of the film, profile of photo-excited mechanical stress, despite the long electron diffusion lengths mentioned earlier.

As expected from SPR-theory, the 45 nm sample shows the highest signal amplitude. Compared to our measurements conducted in direct reflection, where the oscillation of the 45 nm film could not be resolved within $\Delta R/R \leq 2{\cdot}10^{-7}$ sensitivity, we observe a signal enhancement of more than 50 in the plasmonic sensing scheme. To prevent low frequency contributions at longer time delays from distorting our data analysis, we crop the time domain data accordingly. The acoustic signals are then fit with the sum of two exponentially decaying sine functions

$$f(t) = A_1 \exp(-t/\tau_1)\sin(2\pi f_1 t + \Phi_1) + A_3 \exp(-t/\tau_3)\sin(2\pi f_3 t + \Phi_3) + bt + c \quad (1)$$

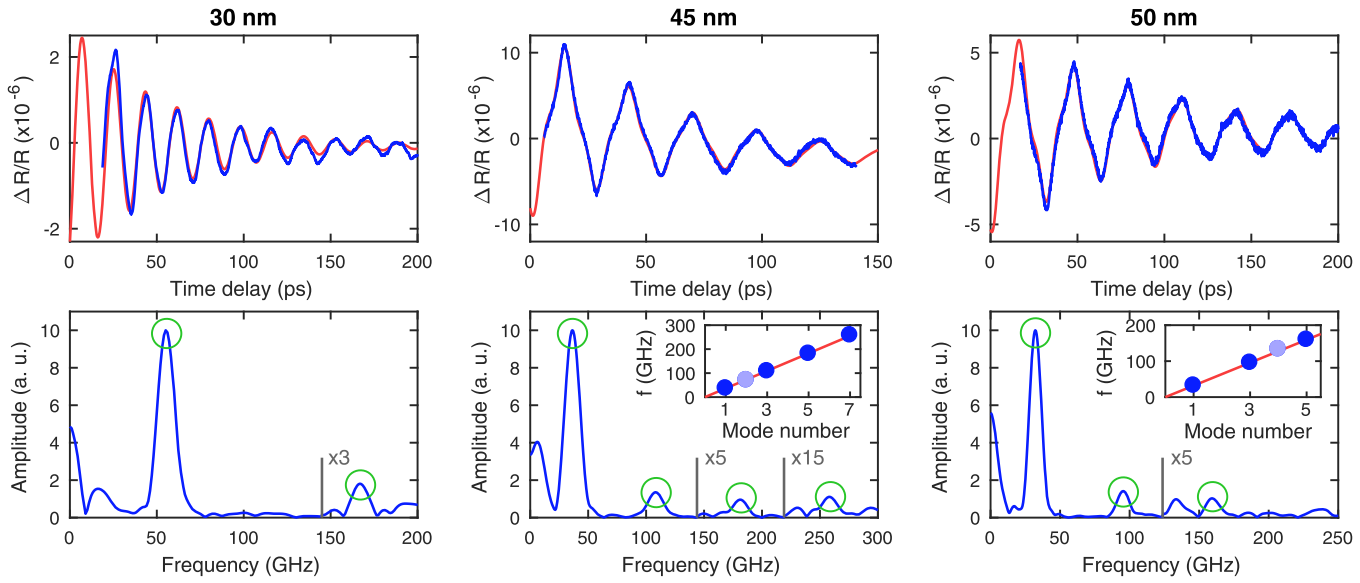

Fig. 5. Upper row: Acoustic contributions in the time domain signal (blue) of the three samples and respective fits (red). Lower row: Corresponding Fourier spectra with odd harmonics of the thickness oscillation (green circles). The Insets show a linear fit to the mode frequency of the odd mode numbers.

with the amplitudes A_i, frequencies f_i, damping times τ_i and phases Φ_i of the first and third harmonic. Additional linear and constant terms were added to compensate for remaining residuals of the signal extraction. The damped sine functions are shown as solid red lines in the upper row of Fig. 5 and fit remarkably well to the 45 nm and 50 nm signals with still very good agreement with the 30 nm signal. The spectra of the complete time traces, which are not shown, also exhibit a common mode at 16.8 GHz. This feature is in good agreement with the expected time-domain Brillouin-scattering at 17.1 GHz in the prism calculated according to [33]. We will now first turn to a discussion of the obtained mode lifetimes which will be followed by a more detailed look into the acousto-plasmonic interaction in the applied sensing approach.

3.3. Acoustic mode lifetimes

Previous studies found energy transmission to the substrate to be the main contribution to the damping of longitudinal modes in thin metal films [34,35]. In the case of perfect adhesion between film and substrate, the mode lifetime $\tau_t = 2d\cdot(v_l \ln(r))^{-1}$ depends only on the layer thickness d, longitudinal sound velocity v_l and reflection coefficient r which is derived from the acoustic impedance mismatch. In particular, the lifetime is independent of the mode number n [36]. Alternatively, the quality factor $Q_{t,n} = n\pi\cdot(\ln(r))^{-1}$ which is independent of the layer thickness but depends on the mode number, can be investigated. Under omission of other damping mechanisms, both transmissive lifetime and Q-factor therefore pose an upper limit to the expected experimental values. Thus, getting experimental access to higher order modes by harnessing plasmonic enhancement effects could be beneficial to investigate and potentially disentangle intrinsic and interface effects on the acoustic damping.

Figure 6 shows the lifetimes and quality factors of the first and third harmonic of the gold films based on the time-domain fits already discussed in Fig. 5. The data points mark the average of one (30 nm), two (50 nm) and three (45 nm) measurements at different spots, detected at the respective angle of maximum enhancement, with the error bars considering all measurements including fitting uncertainties. The third harmonic of the 30 nm sample could not be extracted due to the lower signal enhancement in this sample. The theoretical values for the mode lifetimes, assuming a perfect interface, were calculated with the densities $\varrho_{Au} = 19.3$ g/cm^3 and $\varrho_{NBK7} = 2.51$ g/cm^3 and longitudinal sound velocities $v_{Au} = 3.24$ km/s and $v_{NBK7} = 6.05$ km/s and are indicated by

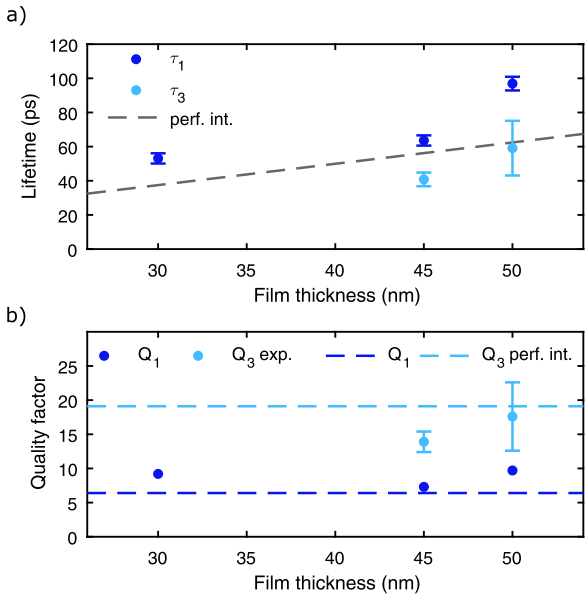

Fig. 6. Lifetimes (a) and quality factors (b) of the fundamental mode (dark blue) and third harmonic (light blue) of the thickness oscillations. The dashed lines mark the expected values according to a perfect interface model. Error bars of Q_1 fall within the marker size and are omitted.

dashed lines.

The fundamental modes of all samples show higher quality factors and longer lifetimes, i.e., lower damping, than expected from the calculations assuming a perfect interface. This corresponds to an increased acoustic reflection coefficient and hints towards a weak adhesion between gold film and prism. This finding is not surprising due to the notorious adhesion issues of gold films on various substrate types and is in agreement with some of our previous work [35,37]. A possible contribution to weak adhesion might be the presence of molecular layers like water vapor that might have been inadvertently embedded during the evaporation process [35,36].

We want to note here that the qualitative observations on transmissive damping do fit the ones on SPR quality: As the damping of the 45 nm sample is closest to theory, this sample seems to have the best

interface quality of the three samples. This is consistent with the strong coupling of light into the SPR that is observed in the measured SPR-curve for this sample. The larger deviation in the damping time of the fundamental mode of the 50 nm sample as well as the observed weak SPR coupling could be explained by weak adhesion. The 30 nm film falls in between the others regarding both values.

In contrast to the findings of the fundamental acoustic mode, the third harmonics exhibit a higher damping compared to values derived for perfect interface adhesion. This hints to the presence of a frequency dependent interface coupling or additional damping mechanisms. The latter could originate from surface roughness [38,39], intrinsic material damping [40], or scattering losses caused by polycrystallinity [41,42]. A possible source of frequency dependent interface coupling would be a "patched" interface as it occurs in nanogranular films or with small scale intermittent adhesion quality. In contrast to our results, however, the theory predicts higher relative lifetimes for higher order modes [43]. The influence in our experiment seems therefore limited or dominated by other effects. However, with the access to several modes, the detection in SPR might be a promising tool for investigation of this topic.

To further explore the potential of this method in the investigation of acoustic damping mechanisms, an improved control in the fabrication and complementary characterization of the deposited layers will be beneficial. We also want to emphasize here that the influence of the cooling of the lattice during the time of the film oscillation ($\approx$ 300 ps) and the accompanying shift of the SPR should be considered in the data evaluation, because the enhancement factor and thus the signal amplitude of the acoustic mode depends on the position of the SPR. The changing enhancement factor during the oscillation might therefore lead to a systematic over- or underestimation of the damping time. However, we observe only small changes in the damping times across the probe incidence angles except for the SPR fringe at very large positive angles, where τ_1 decreases by about 10 % (not shown). Thus, according to our results, this effect plays only a minor role at the angle of measurement for the damping times. Quantifying this contribution will, however, require a more detailed theoretical description of the acousto-plasmonic interaction and lattice thermalization and is beyond the current scope of this work.

3.4. Disentangling contributions to SPR-based detection

We performed a series of measurements on the 45 nm sample with different detection angles, i.e., at different points on the SPR-curve. Since only the position of the slit within the reflected beam was changed and the measurements were taken at the same position and under otherwise identical experimental conditions, all observed variations are a direct consequence of the angle dependent detection process. This method can potentially be used to disentangle the time-resolved contributions of the real and imaginary part of the dielectric function to the signal, as has been demonstrated for the electron dynamics following optical excitation [44–47]. A selection of the extracted acoustic signals is shown in Fig. 7. Three main effects of the detection angle on the signals are visible: an influence on amplitudes, a phase jump of about π close to the SPR angle and a change in signal shape. For angles far off the SPR, the amplitudes of the signals strongly decrease which is a result of the smaller signal enhancement. This also corroborates that possible optical Fabry-Perot effects in the gold film can be neglected and the acoustically induced changes in the SPR dominate our detection process. These basic observations on amplitude and phase are in agreement with previous studies [15,16].

For a more detailed analysis, the parameters of the fundamental mode and third harmonic were determined by fitting damped sine functions to the signals. Since we are interested in a comparison between mode amplitudes and estimates of the thickness changes of the gold film, the respective amplitudes are defined as the value of the decaying envelope at the time t_a of the beginning of the acoustic oscillation (see inset in Fig. 8). The extracted acoustic amplitudes over the detection angle

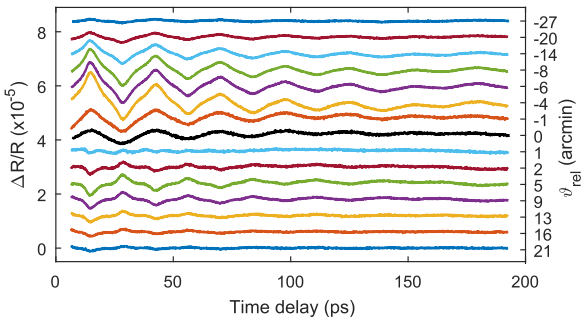

Fig. 7. Overview of the acoustic signals obtained under various angles of detection. The black trace corresponds to the signal at the SPR minimum.

relative to the experimentally observed minimum of the SPR are shown in Fig. 8. The signals with inverted phase are depicted with a negative amplitude for better comparison with the theoretical angle dependent curves. We first focus on the fundamental mode (n = 1). Comparison with Fig. 1 shows a good qualitative agreement with the curves of $(\mathrm{d}R/\mathrm{d}\epsilon_\mathrm{r})$ or $-(\mathrm{d}R/\mathrm{d}d)$. It can already be concluded from the symmetry of the amplitude as a function of detection angle that the imaginary part of the dielectric function plays a limited role in the measured acoustic signal.

To further disentangle and quantify the respective contributions of changes in the parameters, we fit a combination of the theoretical angle dependent functions for $\mathrm{d}R/\mathrm{d}\epsilon_\mathrm{r}$, $\mathrm{d}R/\mathrm{d}\epsilon_\mathrm{i}$, and $\mathrm{d}R/\mathrm{d}d$ to the experimental data. Ideally, the gold layer's permittivity should be determined as precisely as possible to calculate the film dependent derivatives, especially the imaginary part. While small deviations in the absolute value of the real part mostly shift the resonance angle and have limited influence on the behavior relative to the minimum, the absolute value of the imaginary part strongly influences the behavior of $\mathrm{d}R/\mathrm{d}\epsilon_\mathrm{i}$ around the resonance minimum. In particular the imaginary part is known to vary strongly with film quality and evaporation parameters [29]. In principle, the permittivity can be determined by fitting to the static SPR curves (Fig. 3). However, our fit-determined value of $\epsilon_\mathrm{i} = 0.8 \pm 0.2\mathrm{i}$ for the 45 nm film is unrealistically low, compared to the already low $\epsilon_\mathrm{i} = 1.0\mathrm{i}$ which was reached under ideal conditions [29]. Most reported values for the imaginary part at 785 nm fall in the range of $\epsilon_\mathrm{i} = 1.2\mathrm{i} - 1.8\mathrm{i}$ [48]. We therefore use $\epsilon = -22.9 + 1.4\mathrm{i}$ [24] as a reasonable estimate. Please note that, due to the high repetition rate, we cannot rule out heat accumulation effects of a few Kelvin in the samples that might cause a constant background in our measurements.

As mentioned earlier, the finite slit width in our setup introduces an average over 10′ and leads to the effective detection of $\overline{\Delta R}/\overline{R}$. This is considered by applying a moving average to the theoretical curves before fitting. We approximate the variation of the resonance curve by a linear combination of the individual derivatives:

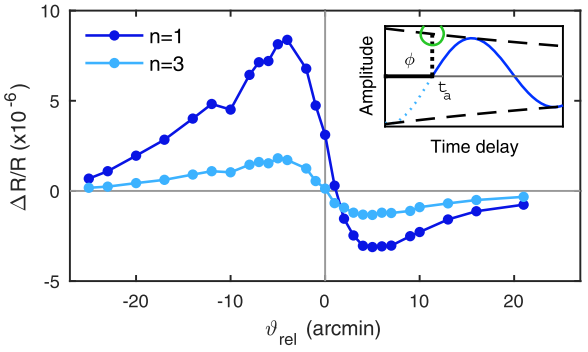

Fig. 8. Extracted amplitudes of the fundamental mode (dark blue) and third harmonic (light blue) of the thickness oscillation. Inset: Sketch of the definition of the acoustic amplitude (green circle).

$$\frac{\overline{\Delta R}}{\overline{R_0}} = \frac{\overline{\Delta R(\Delta\epsilon_{r,i}, \Delta d)}}{\overline{R_0}} \approx \frac{\overline{\Delta R(\Delta\epsilon_r)} + \overline{\Delta R(\Delta\epsilon_i)} + \overline{\Delta R(\Delta d)}}{\overline{R_0}}$$
$$\approx \frac{\Delta\epsilon_r \cdot \overline{dR/d\epsilon_r} + \Delta\epsilon_i \cdot \overline{dR/d\epsilon_i} + \Delta d \cdot \overline{dR/dd}}{\overline{R_0}} \quad (2)$$

The error in $\Delta R/R$ introduced by regarding the variations as independent of each other is less than 10^{-9} in our case and negligible. This linear combination is then least-squares-fitted to the experimental data. Figure 9 shows the obtained fit as solid red line and the individual contributions from variations of the permittivity and thickness as annotated lines. Please note, that their contribution to the detected signal of $\Delta R/R$ is shown, not the absolute variations of the three parameters nor the derivatives of R with respect to these parameters (as in Fig. 1).

We achieve the best fit result for the combination $\Delta\epsilon_r = +1{\cdot}10^{-5}$, $\Delta\epsilon_i = -3{\cdot}10^{-6}$ and $\Delta d = +0.04$ pm, with positive Δd corresponding to an expansion of the gold film. This is in agreement with a positive photoelastic coefficient $\partial\epsilon_r/\partial\eta$, i.e., extensional strain in gold leads to an increase in the real part of the permittivity, as it is expected by an analysis of the Drude-model for energies below the interband transition [20]. Our result further indicates that the effect of strain on the real part of the permittivity is dominant. This is in agreement with reports on acoustic pulses in gold [20] and silver films [49] where only a small variation of the imaginary part was found. However, close to the resonance angle, small variations of the imaginary part can lead to a substantial contribution to the signal of $\Delta R/R$ because of the vanishing background reflectance R. We also note that the accuracy of our experiment regarding the contribution of the imaginary part is limited (see discussion below). The result also corroborates, that the variation of the film thickness, although in the range of only tens of femtometers, cannot be neglected in the SPR detection scheme for planar sample geometries. The contribution of the thickness variation cancels a significant part of the contribution of the real part of the permittivity and, together with the contribution on the imaginary part, causes the asymmetry of the amplitude.

To check the plausibility of the fit result with regard to the thickness variation of the film, we estimate the thermal stress $\sigma = -3\beta(B + 4/3\mu)\Delta T$ due to the absorbed pump energy and subsequent temperature increase $\Delta T = (1-R)\cdot Q/(Ad)\cdot 1/C$ with the linear thermal expansion coefficient $\beta = 14{\cdot}10^{-6}$ 1/K, bulk, B, and shear, μ, moduli $B + 4/3\mu = 260$ GPa, reflectance $R = 0.94$, pulse energy $Q = 0.62$ nJ, illuminated area and film thickness $A = 7.1{\cdot}10^{-10}$ m^2 and $d = 45$ nm and heat capacity $C = 2.5{\cdot}10^6$ J/(m^3 K) [1,50,51]. This yields a change in the gold film thickness of $\Delta d_{est} = +0.3$ pm. The difference of almost an order of magnitude between the experimental value and our theoretical estimation is reasonable, when the same estimate is applied to reported values of the surface displacement [50,52]. Therefore, the applied estimate must be regarded as an upper boundary for the maximum film expansion. It is also important to note that our determined value refers to the fundamental mode only. Because the initial energy is distributed to several acoustic modes, as evidenced by the observed frequency spectra, the actual thickness change caused by the fundamental mode must be below this value.

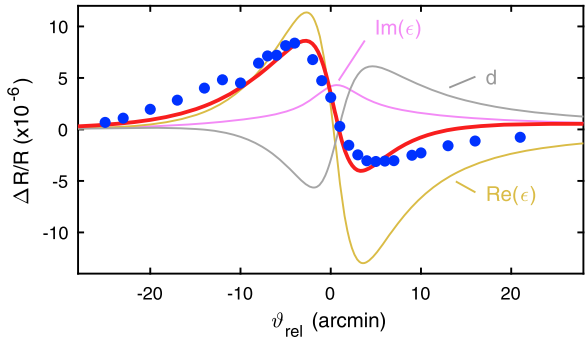

Fig. 9. Measured angle dependent acoustic amplitude of the fundamental mode of the gold film with 45 nm thickness (blue dots) and fitted linear combination of contributions induced by the changes of the gold film's permittivity and thickness (red line). The annotated lines show the contributions of the individual parameters to the fit.

When deducing the dynamics of ϵ and d from the signal amplitude $\Delta R/R$, a possible nonlinear response of the SPR must be considered. Our model assumes the derivative dR/dx with $x = \epsilon_{r,i}, d$ to be constant within the range of induced changes $x_0 \pm \Delta x$. The relative changes of dR/dx in the interval $\pm\Delta x$, with Δx being twice our fit determined values, are less than 10^{-4}. This results in signal deviations of about 10^{-9}. The sole exception of poles at the zero crossings of dR/dx can be as well considered negligible here due to the finite angular detection resolution.

All fits yield results that are narrower than the experimental one. We cannot give a conclusive explanation of this finding yet but identified four potential causes for this behavior: a) the omitted broadening of the plasmon resonance due to the spectral width of our laser pulses, b) a small refraction and broadening of the probe spot at the exit of the prism due to an imperfect or slightly off-center focus of the beam, c) an influence of the sine distribution of strain and therefore $\Delta\epsilon$ within the layer in contrast to the assumed uniform distribution in our calculations and d) the omitted influence of the heating of the film and accompanying possible modification of the permittivity by the absorbed laser power.

The angle dependent amplitude of the third harmonic (light blue in Fig. 8) shows several peculiarities when compared to the fundamental mode. Firstly, the amplitude of the mode exhibits a different zero crossing than the fundamental mode ($\vartheta_{0,n=1} \approx +1'$, $\vartheta_{0,n=3} \approx 0'$). This behavior is already visible in the signal shape of the time domain signals in Fig. 7 where the signals in black (0) and light blue (+1) exhibit almost no contribution of the third harmonic and fundamental mode, respectively. Further, the asymmetry regarding the two sides of the resonance is smaller for the third harmonic than for the fundamental and the relative amplitudes of the two modes show a ratio of 2.5 −4.5 instead of the theoretical expected ratio of 9. We can currently only speculate that this is possibly due to the different strain distributions of the two modes. While our model assumes a uniform, averaged strain and variation of the permittivity over the whole film thickness, the actual distribution follows the respective axial mode profiles. For the third harmonic this leads to regions with opposite sign of the strain and therefore to a partial cancellation of permittivity variations and reduced overall thickness variation of the film. Further, with the exponentially decreasing SP-field amplitude in the gold film it seems reasonable to expect a spatialy inhomogeneous sensitivity function for variations of the permittivity over the film thickness. Since the weighting of the parameters contributes to the asymmetry as well as to the nonzero amplitude at $\vartheta_{rel} = 0$, this might cause the observed differences. In general, an influence of the spatial distribution of the variations can be expected for higher modes. We did not further develop the theory behind the detection of higher harmonics in the planar SPR-scheme yet, but want to note, that also the phase behavior of the third harmonic differs from the fundamental mode. Figure 10 shows the extracted phases from the angle dependent measurements. Besides a different absolute phase jump at the resonance, there seems to be an additional angle dependency of the phase of the third harmonic within the two sides of the resonance that is not fully explained by fit uncertainties. This emphasizes the need for a more detailed theory to fully understand the acousto-plasmonic interaction of different acoustic modes in this detection scheme.

We want to add here an important information regarding the choice of film thicknesses in this type of sensing scheme that we unfortunately realized very late during our experiments. Although the almost complete coupling to the SPR yields a high signal enhancement for the 45 nm film, it also causes an ambiguous behavior at the SPR angle for changes in the imaginary part and is therefore not well suited to determine the contribution of $dR/d\epsilon_i$ which in turn adds uncertainty to the ratio of all fit parameters. For this particular thickness, slightly different values of d and ϵ_i can lead to a zero crossing and an accompanying sign flip of $dR/$

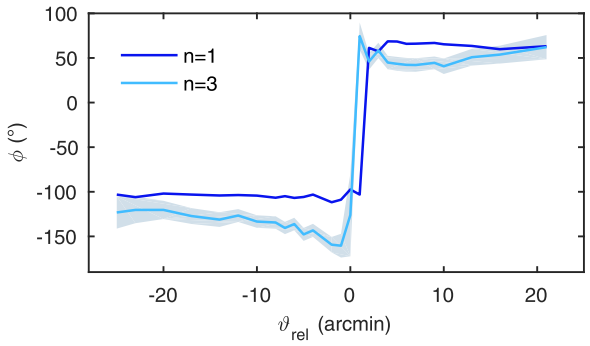

Fig. 10. Extracted phase of the fundamental (dark blue) and third harmonic (light blue). The shaded area depicts the uncertainty of the third harmonic. The uncertainty of the fundamental is omitted for the sake of clarity.

$d\epsilon_i$ at the SPR angle ($\vartheta_{rel} = 0$). Hence, we recommend a film thickness that is a few nanometers off the "optimal" thickness to ensure a well-determined sign of $(dR/d\epsilon_i)$ and $dR/d\epsilon_i \neq 0$ at the SPR-angle.

4. Conclusion

In conclusion, we have applied a surface plasmon based sensing scheme in combination with femtosecond resolved pump-probe measurements to the excitation and detection of longitudinal acoustic eigenmodes in planar gold films. The Kretschmann configuration was employed to couple the optical detection pulses to the surface plasmon resonances in gold films with thicknesses of 30, 45 and 50 nm. The resulting modulation of the time-resolved reflectance by the acoustic dynamics reveals higher order modes up to the 7th order (258 GHz) for the 45 nm film and lower orders for the other film thicknesses. We find a good qualitative agreement between expected signal enhancement factors for the different film thicknesses and experimental observations which are at least a factor of 50 above traditional reflection experiments based on photoelastic detection in direct reflection. Acoustic mode lifetimes are analyzed for the fundamental and third order modes and discussed critically regarding a possible disentanglement of intrinsic and interface adhesion effects. An analysis of the acousto-plasmonic interaction in the detection process reveals the importance to include the often neglected contribution of film thickness changes in addition to contributions stemming from the dielectric function. We find that the experimental configuration is sensitive to thickness changes in the deep sub-pm regime. Finally, we also discuss some important results regarding the choice of an optimal film thickness in this sensing scheme and open questions that need to be addressed in the further development of this approach.

Declaration of Competing Interest

The authors declare that they have no known competing financial interests or personal relationships that could have appeared to influence the work reported in this paper.

Data Availability

Data will be made available on request.

Acknowledgements and Funding

This work has been supported by the German Research Foundation (DFG) through the SFB 767 and by the project "Zero Defect Manufacturing - Universal surface characterization for process optimization" (ZDM_OmniScan) by the Federal Government of Upper Austria and the European Regional Development Fund (EFRE) in the framework of the EU-program IWB2020 with additional funds from the REACT-EU initiative and is co-financed by research subsidies granted by the Government of Upper Austria (Wi-2021-303205/13-Au).

References

[1] C. Thomsen, H.T. Grahn, H.J. Maris, J. Tauc, Surface generation and detection of phonons by picosecond light pulses, Phys. Rev. B 34 (1986) 4129–4138, https://doi.org/10.1103/PhysRevB.34.4129.
[2] J.H.C. Thomsen, J. Strait, Z. Vardeny, H. Maris, J. Tauc, Coherent phonon generation and detection by picosenscond light pulses, Phys. Rev. Lett. 53 (1984) 3–6, https://doi.org/10.1103/PhysRevLett.53.989.
[3] O. Matsuda, M.C. Larciprete, R. Li Voti, O.B. Wright, Fundamentals of picosecond laser ultrasonics, Ultrasonics 56 (2015) 3–20, https://doi.org/10.1016/j.ultras.2014.06.005.
[4] T. Tachizaki, T. Muroya, O. Matsuda, Y. Sugawara, D.H. Hurley, O.B. Wright, Scanning ultrafast Sagnac interferometry for imaging two-dimensional surface wave propagation, Rev. Sci. Instrum. 77 (2006) 43712–43713. http://link.aip.org/link/?RSI/77/043713/1.
[5] D.H. Hurley, O.B. Wright, Detection of ultrafast phenomena by use of a modified Sagnac interferometer, Opt. Lett. 24 (1999) 1305–1307. http://ol.osa.org/abstract.cfm?URI=ol-24-18-1305.
[6] B. Perrin, C. Rossignol, B. Bonello, J.C. Jeannet, Interferometric detection in picosecond ultrasonics, Phys. B Condens. Matter 263–264 (1999) 571–573. https://doi.org/10.1016/S0921-4526(98)01479-3.
[7] A. Bruchhausen, R. Gebs, F. Hudert, D. Issenmann, G. Klatt, A. Bartels, O. Schecker, R. Waitz, A. Erbe, E. Scheer, J.-R. Huntzinger, A. Mlayah, T. Dekorsy, Subharmonic resonant optical excitation of confined acoustic modes in a free-standing semiconductor membrane at GHz frequencies with a high-repetition-rate femtosecond laser, Phys. Rev. Lett. 106 (2011) 1–4, https://doi.org/10.1103/PhysRevLett.106.077401.
[8] O. Wright, K. Kawashima, Coherent phonon detection from ultrafast surface vibrations, Phys. Rev. Lett. 69 (1992) 1668–1671, https://doi.org/10.1103/PhysRevLett.69.1668.
[9] C. Giannetti, B. Revaz, F. Banfi, M. Montagnese, G. Ferrini, F. Cilento, S. Maccalli, P. Vavassori, G. Oliviero, E. Bontempi, L.E. Depero, V. Metlushko, F. Parmigiani, Thermomechanical behavior of surface acoustic waves in ordered arrays of nanodisks studied by near-infrared pump-probe diffraction experiments, Phys. Rev. B 76 (2007), 125413. http://link.aps.org/abstract/PRB/v76/e125413.
[10] A.A. Maznev, K.A. Nelson, T. Yagi, Impulsive stimulated thermal scattering for sub-micron-thickness film characterization, Thin Solid Films 290–291 (1996) 294–298, https://doi.org/10.1016/S0040-6090(96)09015-3.
[11] C. Lee, B. Lawrie, R. Pooser, K.G. Lee, C. Rockstuhl, M. Tame, Quantum plasmonic sensors, Chem. Rev. 121 (2021) 4743–4804, https://doi.org/10.1021/acs.chemrev.0c01028.
[12] A. Crut, P. Maioli, N. Del Fatti, F. Vallée, Optical absorption and scattering spectroscopies of single nano-objects, Chem. Soc. Rev. 43 (2014) 3921–3956, https://doi.org/10.1039/c3cs60367a.
[13] A.L. Tchebotareva, P.V. Ruijgrok, P. Zijlstra, M. Orrit, Probing the acoustic vibrations of single metal nanoparticles by ultrashort laser pulses, Laser Photonics Rev. 4 (2010) 581–597, https://doi.org/10.1002/lpor.200910034.
[14] M. van Exter, A. Lagendijk, Ultrashort surface-plasmon and phonon dynamics, Phys. Rev. Lett. 60 (1988) 49–52, https://doi.org/10.1103/PhysRevLett.60.49.
[15] J. Wang, J. Wu, C. Guo, Resolving dynamics of acoustic phonons by surface plasmons, Opt. Lett. 32 (2007) 719, https://doi.org/10.1364/ol.32.000719.
[16] J. Wang, C. Guo, Effect of electron heating on femtosecond laser-induced coherent acoustic phonons in noble metals, Phys. Rev. B - Condens. Matter Mater. Phys. 75 (2007) 2–6, https://doi.org/10.1103/PhysRevB.75.184304.
[17] S.Y, T. Tahara, Coherent acoustic phonons in a thin gold film probed by femtosecond surface plasmon resonance, J. Raman Spectrosc. 38 (2007) 1538–1553. https://doi.org/10.1002/jrs.2078.
[18] G. De Haan, E. Abram, T.J. Van Den Hooven, P.C.M. Planken, Plasmonic enhancement of photoacoustic strain-waves on gold gratings, AIP Adv. 12 (2022), https://doi.org/10.1063/5.0070630.
[19] G. de Haan, V. Verrina, A.J.L. Adam, H. Zhang, P.C.M. Planken, Plasmonic enhancement of photoacoustic-induced reflection changes, Appl. Opt. 60 (2021) 7304, https://doi.org/10.1364/ao.432659.
[20] V.V. Temnov, C. Klieber, K.A. Nelson, T. Thomay, V. Knittel, A. Leitenstorfer, D. Makarov, M. Albrecht, R. Bratschitsch, Femtosecond nonlinear ultrasonics in gold probed with ultrashort surface plasmons, Nat. Commun. 4 (2013) 1468, https://doi.org/10.1038/ncomms2480.
[21] M. Yamamoto. Surface plasmon resonance (SPR) theory: Tutorial, Department of Energy and Hydrocarbon Chemistry, Kyoto University, 2008. http://www.chem.konan-u.ac.jp/applphys/web_material/spr_tutorial/sprtheory_English.pdf.
[22] E. Kretschmann, Die Bestimmung optischer Konstanten von Metallen durch Anregung von Oberflächenplasmaschwingungen, Z. Für Phys. A Hadron. Nucl. 241 (1971) 313–324, https://doi.org/10.1007/BF01395428.
[23] E. Kretschmann, H. Raether, Radiative decay of non radiative surface plasmons excited by light, Z. für Naturforsch. - Sect. A J. Phys. Sci. 23 (1968) 2135–2136, https://doi.org/10.1515/zna-1968-1247.
[24] P.B. Johnson, R.W. Christy, Optical constants of the noble metals, Phys. Rev. B 6 (1972) 4370–4379, https://doi.org/10.1103/PhysRevB.6.4370.
[25] A.G. Schott, Datasheet N-BK7 517642.251, 2022. https://www.schott.com/shop/advanced-optics/de/Optisches-Glas/N-BK7/c/glass-N-BK7.

[26] R. Gebs, G. Klatt, C. Janke, T. Dekorsy, A. Bartels, High-speed asynchronous optical sampling with sub-50 fs time resolution, Opt. Express 18 (2010) 5974–5983, https://doi.org/10.1364/OE.18.005974.
[27] A. Bartels, R. Cerna, C. Kistner, A. Thoma, F. Hudert, C. Janke, T. Dekorsy, Ultrafast time-domain spectroscopy based on high-speed asynchronous optical sampling, Rev. Sci. Instrum. 78 (2007), https://doi.org/10.1063/1.2714048.
[28] N. Krauß, A. Nast, D.C. Heinecke, C. Kölbl, H.G. Barros, T. Dekorsy, Fiber-coupled high-speed asynchronous optical sampling with sub-50 fs time resolution, Opt. Express 23 (2015) 2145, https://doi.org/10.1364/oe.23.002145.
[29] K.M. Mcpeak, S.V. Jayanti, S.J.P. Kress, S. Meyer, S. Iotti, A. Rossinelli, D.J. Norris, Plasmonic films can easily be better: Rules and recipes, ACS Photonics 2 (3) (2015) 326–333, https://doi.org/10.1021/ph5004237.
[30] O.B. Wright, V.E. Gusev, Ultrafast acoustic phonon generation in gold, Phys. B: Condens 220 (1996) 770–772. https://doi.org/10.1016/0921-4526(95)00880-2.
[31] J. Hohlfeld, S. Wellershoff, J. Gudde, U. Conrad, V. Jahnke, E. Matthias, Electron and lattice dynamics following optical excitation of metals, Chem. Phys. (2000) 237–258, https://doi.org/10.1016/S0301-0104(99)00330-4.
[32] M. Schubert, M. Grossmann, C. He, D. Brick, P. Scheel, O. Ristow, V. Gusev, T. Dekorsy, Generation and detection of gigahertz acoustic oscillations in thin membranes, Ultrasonics 56 (2015) 109–115, https://doi.org/10.1016/j.ultras.2014.06.018.
[33] V.E. Gusev, P. Ruello, Advances in applications of time-domain Brillouin scattering for nanoscale imaging, Appl. Phys. Rev. 5 (2018), 031101, https://doi.org/10.1063/1.5017241.
[34] G. Tas, J.J. Loomis, H.J. Maris, A.A. Bailes III, L.E. Seiberling, Picosecond ultrasonics study of the modification of interfacial bonding by ion implantation, Appl. Phys. Lett. 72 (1998) 2235–2237, doi: https://doi.org/10.1063/1.121276.
[35] M. Hettich, A. Bruchhausen, S. Riedel, T. Geldhauser, S. Verleger, D. Issenmann, O. Ristow, R. Chauhan, J. Dual, A. Erbe, E. Scheer, P. Leiderer, T. Dekorsy, Modification of vibrational damping times in thin gold films by self-assembled molecular layers, Appl. Phys. Lett. 98 (2011) 1–4, https://doi.org/10.1063/1.3604790.
[36] S. Peli, E. Cavaliere, G. Benetti, M. Gandolfi, M. Chiodi, C. Cancellieri, C. Giannetti, G. Ferrini, L. Gavioli, F. Banfi, Mechanical properties of Ag nanoparticle thin films synthesized by supersonic cluster beam deposition, J. Phys. Chem. C 120 (2016) 4673–4681, https://doi.org/10.1021/acs.jpcc.6b00160.
[37] M. Hettich, K. Jacob, O. Ristow, C. He, J. Mayer, M. Schubert, V. Gusev, A. Bruchhausen, T. Dekorsy, Imaging of a patterned and buried molecular layer by coherent acoustic phonon spectroscopy, Appl. Phys. Lett. 101 (2012), 191606, https://doi.org/10.1063/1.4767141.
[38] A.A. Maznev, Boundary scattering of phonons: specularity of a randomly rough surface in the small-perturbation limit, Phys. Rev. B - Condens. Matter Mater. Phys. 91 (2015) 1–9, https://doi.org/10.1103/PhysRevB.91.134306.
[39] D. Gelda, M.G. Ghossoub, K. Valavala, J. Ma, M.C. Rajagopal, S. Sinha, Specularity of longitudinal acoustic phonons at rough surfaces, Phys. Rev. B 97 (2018) 45429, https://doi.org/10.1103/PhysRevB.97.045429.
[40] A.B. Pippard, CXXII. Ultrasonic attenuation in metals, London Edinburgh Dublin Philos. Mag. J. Sci. 46 (1955) 1104–1114, https://doi.org/10.1080/14786441008521122.
[41] M. Su, B. Ostovar, N. Gross, J.E. Sader, W. Chang, S. Link, Acoustic Vibrations and Energy Dissipation Mechanisms for Lithographically Fabricated Plasmonic Nanostructures Revealed by Single-Particle Transient Extinction, Spectroscopy, J. Phys. Chem. C (2021), https://doi.org/10.1021/acs.jpcc.0c09782.
[42] C. Yi, M.N. Su, P.D. Dongare, D. Chakraborty, Y.Y. Cai, D.M. Marolf, R.N. Kress, B. Ostovar, L.J. Tauzin, F. Wen, W.S. Chang, M.R. Jones, J.E. Sader, N.J. Halas, S. Link, Polycrystallinity of lithographically fabricated plasmonic nanostructures dominates their acoustic vibrational damping, Nano Lett. 18 (2018) 3494–3501, https://doi.org/10.1021/acs.nanolett.8b00559.
[43] G. Rizzi, G. Benetti, C. Giannetti, L. Gavioli, F. Banfi, Analytical model of the acoustic response of nanogranular films adhering to a substrate, Phys. Rev. B 104 (2021) 1–15, https://doi.org/10.1103/PhysRevB.104.035416.
[44] A. Devižis, V. Vaičikauskas, V. Gulbinas, Ultrafast pump-probe surface plasmon resonance spectroscopy of thin gold films, Appl. Opt. 45 (2006) 2535–2539, https://doi.org/10.1364/AO.45.002535.
[45] A. Devižis, V. Gulbinas, Ultrafast dynamics of the real and imaginary permittivity parts of a photoexcited silver layer revealed by surface plasmon resonance, Appl. Opt. 47 (2008) 1632–1637, https://doi.org/10.1364/AO.47.001632.
[46] L.A. Nurtdinova, A.V. Petrov, I.V. Yanilkin, A.I. Gumarov, R.V. Yusupov, Ultrafast plasmon resonance modification in epitaxial silver film, Bull. Russ. Acad. Sci. Phys. 86 (2022) 696–700, https://doi.org/10.3103/S1062873822060193.
[47] R.H.M. Groeneveld, R. Sprik, A. Lagendijk, Ultrafast relaxation of electrons probed by surface plasmons at a thin silver film, in, Proceedings of the XVII Int. Conf. Quantum Electron. Dig. 64 (1990) 104–105. https://doi.org/10.1007/978-3-642-84269-6_112.
[48] R.L. Olmon, B. Slovick, T.W. Johnson, D. Shelton, S. Oh, G.D. Boreman, M. B. Raschke, Optical dielectric function of gold, Phys. Rev. B 235147 (2012) 1–9. https://doi.org/10.1103/PhysRevB.86.235147.
[49] N. Del Fatti, C. Voisin, D. Christofilos, F. Vallée, C. Flytzanis, Acoustic vibration of metal films and nanoparticles, J. Phys. Chem. A 104 (2000) 4321–4326, https://doi.org/10.1021/jp994051y.
[50] O.B. Wright, Ultrafast nonequilibrium stress generation in gold and silver, Phys. Rev. B 49 (1994) 9985–9988, https://doi.org/10.1103/PhysRevB.49.9985.
[51] P. Ruello, V.E. Gusev, Physical mechanisms of coherent acoustic phonons generation by ultrafast laser action, Ultrasonics 56 (2015) 21–35, https://doi.org/10.1016/j.ultras.2014.06.004.
[52] O.B. Wright, Y. Sugawara, O. Matsuda, M. Takigahira, Y. Tanaka, S. Tamura, V. E. Gusev, Real-time imaging and dispersion of surface phonons in isotropic and anisotropic materials, Phys. B Condens. Matter 316–317 (2002) 29–34, https://doi.org/10.1016/S0921-4526(02)00421-0.

Felix Noll obtained his Master's Degree in physics in 2016 at the University of Konstanz, Germany. He continued his work in Konstanz in the fields of stimulated Raman scattering and single molecule spectroscopy. In 2021 he joined the Research Center for Non-Destructive Testing (RECENDT GmbH) in Linz, Upper Austria. Current research interests include photoacoustic phenomena with a focus on (picosecond) laser ultrasonics and the development of techniques for non-destructive testing and metrology based on these principles.

Nico Krauß received his Ph.D. in physics 2016 from the University of Konstanz, Germany. His scientific focus was the development of gigahertz asynchronous optical sampling techniques and their applications in metrology using picosecond ultrasonics. After his Ph.D. he joined LaserQuantum GmbH as a product manager, responsible for the 80 MHz femtosecond oszillator product line. In 2018 he joined Carl Zeiss SMT GmbH as a project lead in the metrology department. Since 2022 he is group leader in the metrology department at Carl ZEISS SMT GmbH. His current focus is the development of metrology tools for deep ultraviolet and extreme ultraviolet lithography lenses.

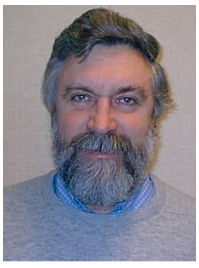

Vitalyi E. Gusev received his PhD degree in physics and mathematics (laser physics) in 1982 from M. V. Lomonosov Moscow State University, Russia. He received Habilitations in Moscow State University in mathematics and physics (acoustics) in 1992 and in Le Mans University, France, in 1997. He is currently a Professor at Le Mans University. Since 1980, his research interests were in the development of the theoretical foundations of nonlinear acoustic, optoacoustic, photothermal and thermoacoustic phenomena. His most recent research has focused on applications of time-domain Brillouin scattering for imaging, on nonlinear laser ultrasonics, acoustics of granular media and nondestructive testing and evaluation of nanomaterials and nanostructures.

Thomas Dekorsy received his Ph.D. from the RWTH Aachen, Germany, in the field of femtosecond spectroscopy of quantum phenomena in semiconductors in 1996. He became Division Head at the Helmholtz Center Dresden-Rossendorf (2000–2005). From 2005 to 2016 he was Professor at University of Konstanz working on high-speed asynchronous optical sampling, ultrafast photo-acoustics, and THz technology. Since 2016 he is Director of the Institut of Technical Physics of the German Aerospace Center (DLR) and Professor at University of Stuttgart with the focus on development of laser systems for aerospace applications. He is fellow of Optica.

Mike Hettich received his Ph.D. degree in physics in 2013 from the University Konstanz, Germany. He continued his studies as postdoctoral fellow at Université Claude Bernard, Lyon 1, Villeurbanne, France until 2015 and returned for another postdoc to University Konstanz until 2018. In 2018 he joined the Research Center for Non-Destructive Testing (RECENDT GmbH) in Linz, Austria, as head of the physical and computational acoustics department. Since 2021 he is the lead scientist of the acoustics area in the RECENDT. His research interests cover the application of picosecond ultrasonics and other laser-based ultrasound methods for non-destructive testing and material characterization from the nano- to the macroscale.